Journal of Solid Mechanics Vol. 13, No. 3 (2021) pp. 305-324
DOI:10.22034/jsm.2020.1889563.1535

Free Vibration Analysis of Composite Grid Stiffened Cylindrical Shells Using A Generalized Higher Order Theory

H. Mohammad Panahiha, A. Davar, M. Heydari Beni , J. Eskandari Jam*

University Complex of Materials and Manufacturing Technology, Malek Ashtar University of Technology, Tehran, Iran

Received 8 June 2021; accepted 2 August 2021

ABSTRACT

The present study analyzes the free vibration of multi-layered composite cylindrical shells and perforated composite cylindrical shells via a modified version of Reddy's third-order shear deformation theory (TSDT) under simple support conditions. An advantage of the proposed theory over other high-order theories is the inclusion of the shell section trapezoidal form coefficient term in the displacement field and strain equations to improve the accuracy of results. The non-uniform stiffness and mass distributions across reinforcement ribs and the empty or filled bays between the ribs in perforated shells were addressed via a proper distribution function. For integrated perforated cylindrical shells, the results were validated by comparison to other studies and the numerical results obtained via ABAQUS. The proposed theory was in good consistency with numerical results and the results of previous studies. It should be noted that the proposed theory was more accurate than TSDT.

Keywords: Free vibration; Grid stiffened cylindrical shell; Natural frequency; Reddy's higher order shell theory.

1 INTRODUCTION

IT is of great importance to analyze perforated structures in mechanical engineering. Designing an analytical model with almost no defects for perforated shells helps obtain appropriate static and dynamic solutions. It is worth noting that the main difference between perforated shells and integrated shells is the grids of the shells, which is essential in analytical modeling. It is crucial to study the static and dynamic behavior of composite structures under different loads in light of their wide range of applications. It seems to be necessary to analyze the vibration of such structures to prevent resonance phenomenon-caused destruction and identify the natural frequencies and different mode shapes. Hence, many researchers studied the free vibration of shells via various analytical, numerical, and experimental methods. Among analytical methods, high-order theories have been adopted in order to analyze thick shells, including composite ones, since high-order theories provide more accurate results. Advanced composite

*Corresponding author. Tel.: +98 9122172195.
E-mail address: jafar.eskandarijam@gmail.com (J.Eskandari Jam)

perforated shells are more complicated to analyze than typical composite shells due to the geometric nature of perforated shells.

The present study's objective is to employ an extended model for perforated cylindrical structures via an equivalent single-layer theory. The entire physical states of a perforated shell are accurately described by a distribution function in the theoretical analysis. Then, the main equations of a perforated shell are obtained by incorporating the main assumptions of the classical plane theory and shell equations.

2 LITRATURE REVIEW

Takabatake (1990) statically and dynamically analyzed cavity shells. The cavity-induced discontinuity changes were described using Hamilton's principle and extended Dirac delta function [1, 2]. It should be noted that they applied a general analysis method to cavity circular shells based on Law's assumptions and incorporating the bending stiffness distribution of a cavity plan by a specific function. Lee et al. (2011) used a new computational method for the vibration of isotropic cavity rectangular planes. They employed the static functions of a beam under a point load. Also, the Rayleigh-Ritz method was used to analyze the variation of the plane's discontinuities [3]. Huybrechts (1996) employed computer codes by proposing a deformation model of a perforated structure in the fracture space. Various perforated structures with different shapes were parametrically investigated using the codes [4, 5] . Han et al. (2003) introduced a method to manufacture advanced stiffened perforated plane panels. A square grid was produced with fractured joints, glued connections, and pultruded grooves. These technologies led to progress in manufacturing the first large-scale perforated models, dramatically changing the manufacturing of such engineering structures [6]. Jiang (1992) utilized a numerical technique to analyze the free vibration of perpendicularly-reinforced cylindrical shells. The technique was developed in the form of a specific finite element method (FEM). They were able to reduce the response convergence time [7]. Hemmatnejad et al. (2013) studied the vibration behavior of perforated- and wave rib-reinforced cylindrical composite shells. They used impregnation to add the reinforcement stiffening effect to the total stiffness of the shell and calculate the equivalent stiffness [8]. Levan et al. (2011) introduced a new impregnation method to model the vibration of thin shells with intersecting reinforcement. They observed high accuracy by comparing the results to the FEM results [9]. Edalat et al. (2013) studied the dynamic responses of a shell reinforced with parabolic curves. They employed the energy method to determine the equivalent orthotropic parameters [10]. Eskandari Jam et al. (2010) investigated the dynamic behavior of a perforated shell via the shear deformation theory. They compared their results to FEM results. Finally, the variation of the natural frequency by other parameters was provided [11, 12]. Sayyad (2010) analyzed the inter-layer grid shear effect on the local buckling of a perforated polymer composite shell under uniform compressive loading [13]. Li et al. (2019) investigated A Unified Approach of Free Vibration Analysis for Stiffened Cylindrical Shell with General Boundary Conditions [33]. The present study addresses the non-uniform distributions of stiffness and mass among reinforcement rips and their empty or filled bays via a proper distribution function. For integrated and perforated shells, the results were validated by comparing them to the numerical results obtained from ABAQUS and the results provided by previous studies.

3 PROBLEM- SOLVING

3.1 Assumptions

The following assumptions were made in analyzing cylindrical shells and deriving equilibrium equations:

- The thin-wall shell assumptions and Law's first approximation were used,
- The shell's length and diameter were considered as limited,
- The damping effect was ignored,
- The material was assumed to be in the linear-elastic region, and
- Nonlinear terms were excluded.

3.2 Determining displacement components

Fig. 1 illustrates a composite cylindrical shell with the mean radius, thickness, and length of R, h, and L, respectively

along with the reference coordinate system. The middle surface was considered as the reference surface on which the cylindrical coordinate system was fixed [14, 15].

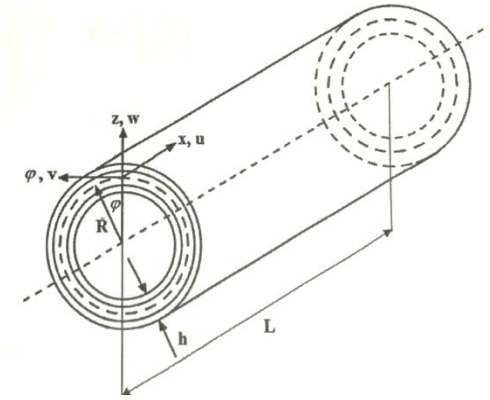

Fig.1
The composite cylindrical shell with the reference coordinate system [16].

$$\begin{aligned} u(x,\varphi,z,t) &= u_0(x,\varphi,t) + z\,\theta_x(x,\varphi,t) + z^2 u_0^*(x,\varphi,t) + z^3\theta_x^*(x,\varphi,t) \\ v(x,\varphi,z,t) &= (1+\gamma_0 z/R)v_0(x,\varphi,t) + z\,\theta_\varphi(x,\varphi,t) + z^2 v_0^*(x,\varphi,t) + z^3\theta_\varphi^*(x,\varphi,t) \\ w(x,\varphi,z,t) &= w_0(x,\varphi,t) \end{aligned} \tag{1}$$

where u, v, and w are the displacement components of point (x,φ,z) in the multi-layer space and t is time. Also, u_0 and v_0 are the in-plane displacement components, while w_0 is the off-plane displacement component on the middle surface. Functions θ_x and θ_φ denote the rotations of the line perpendicular to the middle surface around axes φ and x, respectively. In addition, u_0^*, v_0^*, θ_x^*, and θ_x^* are high-order Taylor series parameters and represent the transverse deformation modes of the shell cross-section, which are defined as:

$$\theta_x = \left.\frac{\partial u}{\partial z}\right|_{z=0} \quad u_0^* = \left.\frac{1}{2}\frac{\partial^2 u}{\partial z^2}\right|_{z=0} \quad \theta_x^* = \left.\frac{1}{6}\frac{\partial^3 u}{\partial z^3}\right|_{z=0} \quad \theta_\varphi = \left.\frac{\partial v}{\partial z}\right|_{z=0} \quad v_0^* = \left.\frac{1}{2}\frac{\partial^2 v}{\partial z^2}\right|_{z=0} \quad \theta_\varphi^* = \left.\frac{1}{6}\frac{\partial^3 v}{\partial z^3}\right|_{z=0} \tag{2}$$

In the proposed theory, the effect of transverse normal strains (along the thickness) on the cylindrical shell surface is assumed to be zero. This assumption simplifies the calculations of the theory and allows for comparing the results to those of other theories.

Replacing the lateral strain Eqs. (1) and making them equal to zero provides a simpler definition of displacement components as:

$$\begin{aligned} \gamma_{xz} &= \frac{\partial u}{\partial z} + \frac{\partial w}{\partial x} \\ \gamma_{\varphi z} &= \left(\frac{1}{R}\frac{\partial w}{\partial \varphi} - \frac{v_0}{R}\right) + \frac{\partial v}{\partial z} \end{aligned} \tag{3}$$

$$\begin{aligned} u_0^* &= v_0^* = 0 \\ \theta_x^* &= \frac{-4}{3h^2}\left(\theta_x + \frac{\partial w_0}{\partial x}\right) \\ \theta_\varphi^* &= \frac{-4}{3h^2}\left(\theta_\varphi + \frac{1}{R}\frac{\partial w_0}{\partial \varphi} - \frac{v_0}{R}\right) \end{aligned} \tag{4}$$

Finally, the displacement components are simplified to [17]:

$$
\begin{aligned}
u(x,\varphi,z,t) &= u_0(x,\varphi,t) + z\,\theta_x(x,\varphi,t) + \frac{-4}{3h^2}(\theta_x + \frac{\partial w_0}{\partial x}) \\
v(x,\varphi,z,t) &= (1+\gamma_0 z/R)v_0(x,\varphi,t) + z\,\theta_\varphi(x,\varphi,t) + \frac{-4}{3h^2}(\theta_\phi + \frac{1}{R}\frac{\partial w_0}{\partial \varphi} - \frac{v_0}{R}) \\
w(x,\varphi,z,t) &= w_0(x,\varphi,t)
\end{aligned}
\tag{5}
$$

The presence of the trapezoidal coefficient must be ensured in the main displacement equations. This was considered in the final programming. The proposed theory was compared to the HOST theory introduced in [17], which did not include the trapezoidal coefficient in the analytical calculations.

3.3 Defining strain-displacement relation

By defining strains from the linear elasticity theory for cylindrical shells, general strain-displacement relations in the cylindrical coordinate system, including the trapezoidal effect, are [18,19]:

$$
\begin{aligned}
\varepsilon_x &= \frac{\partial u}{\partial x} \\
\varepsilon_\varphi &= \left(\frac{1}{R}\frac{\partial v}{\partial \varphi} + \frac{w}{R}\right)\frac{1}{1+\gamma_0 z/R} \\
\varepsilon_z &= 0 \\
\varepsilon_{\varphi x} &= \left(\frac{1}{R}\frac{\partial u}{\partial \varphi}\right)\frac{1}{1+\gamma_0 z/R} \\
\varepsilon_{x\varphi} &= \frac{\partial v}{\partial x} \\
\gamma_{xz} &= \frac{\partial u}{\partial z} + \frac{\partial w}{\partial x} \\
\gamma_{\varphi z} &= \left(\frac{1}{R}\frac{\partial w}{\partial \varphi} - \frac{v}{R}\right)\frac{1}{1+\gamma_0 z/R} + \frac{\partial v}{\partial z}
\end{aligned}
\tag{6}
$$

Replacing the displacements of any point in the multi-layer space in (6) provides the middle surface displacement-based linear strains for any displacement model as:

$$
\begin{aligned}
\varepsilon_x &= \varepsilon_{x_0} + z\,\chi_x + z^2\varepsilon^*_{x_0} + z^3\chi^*_x \\
\varepsilon_\varphi &= \frac{1}{1+\gamma_0 z/R}\left(\varepsilon_{\varphi_0} + z\,\chi_\varphi + z^2\varepsilon^*_{\varphi_0} + z^3\chi^*_\varphi\right) \\
\varepsilon_z &= 0 \\
\gamma_{x\varphi} &= \left(\varepsilon_{x\varphi_0} + z\,\chi_{x\varphi} + z^2\varepsilon^*_{x\varphi_0} + z^3\chi^*_{x\varphi}\right) + \frac{1}{1+\gamma_0 z/R}\left(\varepsilon_{\varphi x_0} + z\,\chi_{\varphi x} + z^2\varepsilon^*_{\varphi x_0} + z^3\chi^*_{\varphi x}\right) \\
\gamma_{xz} &= \beta_x + z\,\chi_{xz} + z^2\beta^*_x + z^3\chi^*_{xz} \\
\gamma_{\varphi z} &= \frac{1}{1+\gamma_0 z/R}(\beta_{\varphi_0} + z\,\chi_{\varphi z_0} + z^2\beta^*_{\varphi_0} + z^3\chi^*_{\varphi z_0}) + (\beta_{\varphi_1} + z\,\chi_{\varphi z_1} + z^2\beta^*_{\varphi_1})
\end{aligned}
\tag{7}
$$

In which γ_0 is the trapezoidal shape effect coefficient of the shell section. It should be noted that the proposed theory considers this coefficient as 1, unlike Reddy's theory [17]. Moreover, the expressions inside parentheses in (7) can be calculated as [20]:

$$
\begin{aligned}
&\varepsilon_{x_0}=\frac{\partial u_0}{\partial x}\ ,\ \chi_x=\frac{\partial \theta_x}{\partial x}\ ,\ \varepsilon^*_{x_0}=0\ ,\ \chi^*_x=(\frac{-4}{3h^2})(\frac{\partial \theta_x}{\partial x}+\frac{\partial^2 w_0}{\partial x^2})\\
&\varepsilon_{\varphi_0}=\frac{1}{R}\frac{\partial v_0}{\partial \varphi}+\frac{w_0}{R}\ ,\ \chi_\varphi=\gamma_0\frac{1}{R^2}\frac{\partial v_0}{\partial \varphi}+\frac{1}{R}\frac{\partial \theta_\varphi}{\partial \varphi}\ ,\ \varepsilon^*_{\varphi_0}=0\ ,\ \chi^*_\varphi=\frac{1}{R}(\frac{-4}{3h^2})(\frac{\partial \theta_\varphi}{\partial \varphi}+\frac{1}{R}\frac{\partial^2 w_0}{\partial \varphi^2}-\frac{1}{R}\frac{\partial v_0}{\partial \varphi})\\
&\varepsilon_{z_0}=0,\ \chi_z=0\ ,\ \varepsilon^*_{z_0}=0\\
&\varepsilon_{x\varphi_0}=\frac{\partial v_0}{\partial x}\ ,\ \chi_{x\varphi}=\gamma_0\frac{1}{R}\frac{\partial v_0}{\partial x}+\frac{\partial \theta_\varphi}{\partial x}\ ,\ \varepsilon^*_{x\varphi_0}=0\ ,\ \chi^*_{x\varphi}=(\frac{-4}{3h^2})(\frac{\partial \theta_\varphi}{\partial x}+\frac{1}{R}\frac{\partial^2 w_0}{\partial x\,\partial \varphi}-\frac{1}{R}\frac{\partial v_0}{\partial x})\\
&\varepsilon_{\varphi x_0}=\frac{1}{R}\frac{\partial u_0}{\partial \varphi}\ ,\ \chi_{\varphi x}=\frac{1}{R}\frac{\partial \theta_x}{\partial \varphi}\ ,\ \varepsilon^*_{\varphi x_0}=0\ ,\ \chi^*_{\varphi x}=\frac{1}{R}(\frac{-4}{3h^2})(\frac{\partial \theta_x}{\partial \varphi}+\frac{\partial^2 w_0}{\partial x\,\partial \varphi})\\
&\beta_x=\theta_x+\frac{\partial w_0}{\partial x}\ ,\ \chi_{xz}=0\ ,\ \beta^*_x=3(\frac{-4}{3h^2})(\theta_x+\frac{\partial w_0}{\partial x})\ ,\ \chi^*_{xz}=0\\
&\beta_{\varphi_0}=\frac{1}{R}\frac{\partial w_0}{\partial \varphi}-\frac{v_0}{R}\ ,\ \chi_{\varphi z_0}=-\gamma_0\frac{v_0}{R^2}-\frac{\theta_\varphi}{R}\ ,\ \beta^*_{\varphi_0}=0\ ,\ \chi^*_{\varphi z_0}=\frac{-1}{R}(\frac{-4}{3h^2})(\theta_\varphi+\frac{1}{R}\frac{\partial w_0}{\partial \varphi}-\frac{1}{R}v_0)\\
&\beta_{\varphi_1}=\gamma_0\frac{v_0}{R}+\theta_\varphi,\quad \chi_{\varphi z_1}=0,\qquad \beta^*_{\varphi_1}=3(\frac{-4}{3h^2})(\theta_\varphi+\frac{1}{R}\frac{\partial w_0}{\partial \varphi}-\frac{1}{R}v_0)
\end{aligned}
\tag{8}
$$

3.4 Defining stress-strain relations in composites and resultant stresses

Assuming the main axes to be defined in the material coordinate system (1, 2, 3) and multi-layer axes (x, φ, z), the 3D stress-strain relations of orthotropic layer k are defined as:

$$
\begin{Bmatrix}\sigma_1\\ \sigma_2\\ 0\\ \tau_{12}\\ \tau_{13}\\ \tau_{23}\end{Bmatrix}^k=\begin{bmatrix}C_{11}&C_{12}&C_{13}&0&0&0\\ C_{12}&C_{22}&C_{23}&0&0&0\\ C_{13}&C_{23}&C_{33}&0&0&0\\ 0&0&0&C_{44}&0&0\\ 0&0&0&0&C_{55}&0\\ 0&0&0&0&0&C_{66}\end{bmatrix}^K\begin{Bmatrix}\varepsilon_1\\ \varepsilon_2\\ 0\\ \gamma_{12}\\ \gamma_{13}\\ \gamma_{23}\end{Bmatrix}^k,\ \varepsilon_3=\sigma_3=0 \tag{9}
$$

where the entries of the stiffness matrix are defined as [15]:

$$
\begin{aligned}
&C_{11}=\frac{E_{11}(1-\nu_{23}\nu_{32})}{\nu^*},C_{12}=\frac{E_{11}(\nu_{21}+\nu_{31}\nu_{23})}{\nu^*},C_{13}=\frac{E_{11}(\nu_{31}+\nu_{21}\nu_{32})}{\nu^*}\\
&C_{22}=\frac{E_{22}(1-\nu_{13}\nu_{31})}{\nu^*},C_{23}=\frac{E_{22}(\nu_{32}+\nu_{12}\nu_{31})}{\nu^*},C_{33}=\frac{E_{33}(1-\nu_{12}\nu_{21})}{\nu^*}\\
&C_{44}=G_{12},C_{55}=G_{13},C_{66}=G_{23}\\
&\nu^*=(1-\nu_{12}\nu_{21}-\nu_{23}\nu_{32}-\nu_{13}\nu_{31}-2\nu_{21}\nu_{32}\nu_{13})
\end{aligned}
\tag{10}
$$

In which G_{ij} is the shear modulus, E_{ij} is the Young modulus, and ν_{ij} is Poisson's ratio. They are not independent of each other but are related as:

$$
\frac{\nu_{12}}{E_{11}}=\frac{\nu_{21}}{E_{22}},\frac{\nu_{13}}{E_{11}}=\frac{\nu_{31}}{E_{33}},\frac{\nu_{23}}{E_{22}}=\frac{\nu_{32}}{E_{33}} \tag{11}
$$

The main material axes of a single layer may not match the main coordinate axes (x, φ, z). Thus, it is required to move the basic relations from single-layer axes (1, 2, 3) to the reference multi-layer axes. The final relations are thus obtained as [15]:

$$\begin{Bmatrix} \sigma_x \\ \sigma_\phi \\ 0 \\ \sigma_{x\phi} \\ \sigma_{xz} \\ \sigma_{\phi z} \end{Bmatrix}^k = \begin{bmatrix} Q_{11} & Q_{12} & Q_{13} & Q_{14} & 0 & 0 \\ Q_{12} & Q_{22} & Q_{23} & Q_{24} & 0 & 0 \\ Q_{13} & Q_{23} & Q_{33} & Q_{34} & 0 & 0 \\ Q_{14} & Q_{24} & Q_{34} & Q_{44} & 0 & 0 \\ 0 & 0 & 0 & 0 & Q_{55} & Q_{56} \\ 0 & 0 & 0 & 0 & Q_{56} & Q_{66} \end{bmatrix}^k \begin{Bmatrix} \varepsilon_x \\ \varepsilon_\phi \\ 0 \\ \gamma_{x\phi} \\ \gamma_{xz} \\ \gamma_{\phi z} \end{Bmatrix}^k , \ \varepsilon_z = 0 \tag{12}$$

or and a summarized form as:

$$\sigma = Q\varepsilon \tag{13}$$

where the matrix coefficients are the elastic coefficients of the orthotropic material of layer *k*, which, considering the arrangement of layers from the inside (*k*=1*)* to the outside (*k=NL)*, are [15]:

$$\begin{aligned}
&Q_{11} = C_{11}c^4 + 2(C_{12} + 2C_{44})s^2c^2 + C_{22}s^4; \\
&Q_{12} = C_{12}(c^4 + s^4) + (C_{11} + C_{22} - 4C_{44})s^2c^2; \\
&Q_{13} = (C_{13}c^2 + C_{23}s^2); \\
&Q_{14} = (C_{11} - C_{12} - 2C_{44})sc^3 + (C_{12} - C_{22} + 2C_{44})s^3c; \\
&Q_{22} = C_{11}s^4 + 2(C_{12} + 2C_{44})s^2c^2 + C_{22}c^4; \\
&Q_{23} = C_{13}s^2 + C_{23}c^2; \\
&Q_{24} = (C_{11} - C_{12} - 2C_{44})s^3c + (C_{12} - C_{22} + 2\mathrm{C}_{44})sc^3; \\
&Q_{33} = C_{33}; \\
&Q_{34} = (C_{31} - C_{32})sc; \\
&Q_{44} = (C_{11} - 2C_{12} + C_{22} - 2C_{44})s^2c^2 + C_{44}(\mathrm{c}^4 + s^4); \\
&Q_{55} = (C_{55}c^2 + C_{66}s^2); \\
&Q_{56} = (C_{55} - C_{66})\,\mathrm{sc}; \\
&Q_{66} = (C_{55}s^2 + C_{66}c^2); \\
&\mathrm{Q}_{ij} = \mathrm{Q}_{ji} \\
&i\,,\mathrm{j} = 1,\ldots,6
\end{aligned} \tag{14}$$

In which *s=sin(θ)*, *c=cos(θ)*, and θ is fiber's orientation. The clockwise orientation of with respect to the fiber angle direction, i.e., the positive *x*-axis direction, is considered as the positive orientation. Replacing (7) and (12) and integrating it in the thickness direction reduces (13) to:

$$\bar{\sigma} = D\bar{\varepsilon} \tag{15}$$

where:

$$D = \begin{bmatrix} D_f & 0 \\ 0 & D_s \end{bmatrix}, D_f = \begin{bmatrix} D_m & D_{mc} \\ D_{bc} & D_b \end{bmatrix} \tag{16}$$

In which D_m , D_{mc} , D_{bc} , D_b , and D_s are the material property matrixes. The components of resultant stress vector $\bar{\sigma}$ and the components of middle surface strain vector $\bar{\varepsilon}$ are defined as:

$$\bar{\sigma} = \left(N_x, N_\varphi, N_{\varphi x}, N_{x\varphi}, N_x^*, N_\varphi^*, N_{\varphi x}^*, N_{x\varphi}^*, N_z, N_z^*, M_x, M_\varphi, M_{\varphi x}, M_{x\varphi}, M_x^*, M_\varphi^*, M_{\varphi x}^*, M_{x\varphi}^*, M_z, Q_x, Q_\varphi, R_\varphi, Q_x^*, Q_\varphi^*, R_\varphi^*, S_x, S_\varphi, T_\varphi, S_x^*, S_\varphi^*\right)^T \tag{17}$$

and

$$\bar{\varepsilon}=\left(\varepsilon_{x_0},\varepsilon_{\varphi_0},\varepsilon_{\varphi x_0},\varepsilon_{x\varphi_0},\varepsilon^*_{x_0},\varepsilon^*_{\varphi_0},\varepsilon^*_{\varphi x_0},\varepsilon^*_{x\varphi_0},\varepsilon_{z_0},\varepsilon^*_{z_0},\chi_x,\chi_\varphi,\chi_{\varphi x},\chi_{x\varphi},\chi^*_x,\chi^*_\varphi,\chi^*_{\varphi x},\chi^*_{x\varphi},\chi_z,\beta_x,\beta_{\varphi_0},\beta_{\varphi_1},\beta^*_x,\beta^*_{\varphi_0},\beta^*_{\varphi_1},\chi_{xz},\chi_{\varphi z_0},\chi_{\varphi z_1},\chi^*_{xz},\chi^*_{\varphi z_0}\right)^T \tag{18}$$

As can be seen in (17) and (18), resultant stress vector $\bar{\sigma}$ and middle surface strain vector $\bar{\varepsilon}$ contain 30 components. As $\varepsilon^*_{x_0},\varepsilon^*_{\varphi_0},\varepsilon^*_{\varphi x_0},\varepsilon^*_{x\varphi_0},\varepsilon_{z_0},\varepsilon^*_{z_0},\chi_x$, χ_z, $\beta^*_{\varphi_0}$, χ_{xz}, $\chi_{\varphi z_1}$, and χ^*_{xz} are zero, they resultants $N^*_x,N^*_\varphi,N^*_{\varphi x},N^*_{x\varphi}$, N_z,N^*_z, M_z, Q^*_φ, S_x, T_φ, and S^*_x are zero, being excluded from the equations. In (15), resultant vector $\bar{\sigma}$ is calculated for *NL* layers as:

$$\begin{bmatrix} N_x & M_x & - & M^*_x \\ N_{x\varphi} & M_{x\varphi} & - & M^*_{x\varphi} \\ Q_x & - & Q^*_x & - \\ R_\varphi & - & R^*_\varphi & - \end{bmatrix}=\sum_{i=1}^{NL}\int_{z_i}^{z_{i+1}}\begin{Bmatrix}\sigma_x\\ \sigma_{x\varphi}\\ \sigma_{xz}\\ \sigma_{\varphi z}\end{Bmatrix}\left(1,z,z^2,z^3\right)\left(1+\frac{\gamma_0 z}{R}\right)dz$$
$$\begin{bmatrix} N_\varphi & M_\varphi & - & M^*_\varphi \\ N_{\varphi x} & M_{\varphi x} & - & M^*_{\varphi x} \\ Q_\varphi & S_\varphi & - & S^*_\varphi \end{bmatrix}=\sum_{i=1}^{NL}\int_{z_i}^{z_{i+1}}\begin{Bmatrix}\sigma_\varphi\\ \sigma_{\varphi x}\\ \sigma_{\varphi z}\end{Bmatrix}\left(1,z,z^2,z^3\right)dz \tag{19}$$

where z_i and z_i+1 are the bays of the inner and outer surfaces from the middle surface, respectively.

3.5 The governing equations

The equations governing a cylindrical shell are derived using Hamilton's principle for dynamic analysis.

3.5.1 Hamilton's principle

The analytical form of Hamilton's principle can be represented as [19]:

$$\delta\int_{t_1}^{t_2}\left[U-K-W\right]dt=0 \tag{20}$$

where *U* is the total energy resulting from deformation, which is defined as:

$$U=\frac{1}{2}\iiint_V\sigma_{ij}\varepsilon_{ij}dV=\frac{1}{2}\int_0^L\int_0^{2\pi}\int_{-h/2}^{h/2}\left[\sigma_x\varepsilon_x+\sigma_\varphi\varepsilon_\varphi+\sigma_{x\varphi}\varepsilon_{\varphi x}+\sigma_{\varphi x}\varepsilon_{x\varphi}+\sigma_{xz}\varepsilon_{xz}+\sigma_{\varphi z}\varepsilon_{\varphi z}\right]dA\,dz \tag{21}$$

In which a shell surface element is defined as [19]:

$$dA=R\,dx\,d\varphi \tag{22}$$

Moreover, *W* in (20) is the potential energy resulting from external forces, which is calculated as:

$$W=W_x+W_0=\int_0^{2\pi}\int_{-h/2}^{h/2}\left[\hat{\sigma}_x u+\hat{\sigma}_{x\varphi}v+\hat{\sigma}_{xz}w\right]\left(1+\frac{\gamma_0 z}{R}\right)R\,d\varphi dz+\int_0^L\int_0^{2\pi}\left[\mathrm{q}w\right]dA \tag{23}$$

where W_x is the work of edge forces on boundaries and W_0 is the work of surface forces. Also, *K* denotes the kinetic energy in (20), which is derived as:

$$K = \frac{1}{2}\iiint_V \rho[\dot{u}^2 + \dot{v}^2 + \dot{w}^2]dV = \frac{1}{2}\int_0^L\int_0^{2\pi}\int_{-h/2}^{h/2} \rho[\dot{u}^2 + \dot{v}^2 + \dot{w}^2]dA\,dz \tag{24}$$

To solve the problem, (20) can be written as:

$$\delta\int_{t_1}^{t_2}\left[U - K - W\right]dt = 0 \tag{25}$$

In which kinetic energy variation is calculated as:

$$\begin{aligned}\int_0^t \delta K dt &= -\int_0^t [\iiint_A \rho(\ddot{u}\,\delta u + \ddot{v}\,\delta v + \ddot{w}\,\delta w)dA]dt \\ &= -\int_0^t \iiint_A \rho \begin{bmatrix} (\ddot{u}_0 + z\,\ddot{\theta}_x + z^3\frac{-4}{3h^2}(\ddot{\theta}_x + \frac{\partial^2 w_0}{\partial t\,\partial x}))\times \\ (\delta u_0 + z\,\delta\theta_x + z^3\delta\frac{-4}{3h^2}(\theta_x + \frac{\partial w_0}{\partial x})) \\ +(\ddot{v}_0(1+\gamma_0 z/R) + z\,\ddot{\theta}_\varphi + z^3\frac{-4}{3h^2}(\ddot{\theta}_\varphi + \frac{1}{R}\frac{\partial^2 w_0}{\partial t\,\partial\varphi} - \frac{\ddot{v}_0}{R}))\times \\ (\delta v_0(1+\gamma_0 z/R) + z\,\delta\theta_\varphi + z^3\delta\frac{-4}{3h^2}(\theta_\varphi + \frac{1}{R}\frac{\partial w_0}{\partial\varphi} - \frac{v_0}{R})) \\ +(\ddot{w}_0)\times(\delta w_0)\end{bmatrix} dA\,dt\end{aligned} \tag{26}$$

and external force-induced potential energy variation is calculated as:

$$\delta W = \int_0^{2\pi}\begin{bmatrix} \hat{N}_x\,\delta u_0 + \hat{M}_x\,\delta\theta_x + \hat{M}_x^*(\frac{-4}{3h^2})\delta\theta_x + \hat{M}_x^*(\frac{-4}{3h^2})\delta\frac{\partial w_0}{\partial x} \\ +\hat{N}_{x\varphi}\,\delta v_0 + \hat{M}_{x\varphi}(\gamma_0/R)\delta\theta_\varphi + \hat{M}_{x\varphi}^*(\frac{-4}{3h^2})\delta\theta_\varphi + \hat{M}_{x\varphi}^*(\frac{-4}{3h^2})\frac{1}{R}\delta\frac{\partial w_0}{\partial\varphi} \\ +\hat{M}_{x\varphi}^*(\frac{-4}{3h^2})\frac{1}{R}\delta v_0 + \hat{Q}_x\,\delta w_0\end{bmatrix}_0^L Rd\varphi + \int_0^L\int_0^{2\pi}[q\,\delta w_0]dA \tag{27}$$

where the integration values in the first integral in the thickness direction (i.e., z) are represented as:

$$\begin{aligned}\left(\hat{N}_x, \hat{M}_x, \hat{M}_x^*\right) &= \int_{-h/2}^{h/2}\sigma_x\left(1, z, z^3\right)(1+\gamma_0 z/R)dz \\ \left(\hat{N}_{x\varphi}, \hat{M}_{x\varphi}, \hat{M}_{x\varphi}^*\right) &= \int_{-h/2}^{h/2}\sigma_{x\varphi}\left(1, z, z^3\right)(1+\gamma_0 z/R)dz \\ \left(Q_x, Q_x^*\right) &= \int_{-h/2}^{h/2}\sigma_{xz}\left(1, z^2\right)(1+\gamma_0 z/R)dz\end{aligned} \tag{28}$$

Strain energy variation is defined as:

$$\int_0^t \delta U dt = \int_0^t \iiint_A \int_{-h/2}^{h/2} \begin{bmatrix} \sigma_x \delta\varepsilon_x + \sigma_\varphi \delta\varepsilon_\varphi + \sigma_{x\varphi} \delta\varepsilon_{\varphi x} \\ \sigma_{x\varphi} \delta\varepsilon_{x\varphi} + \sigma_{xz} \delta\varepsilon_{xz} + \sigma_{\varphi z} \delta\varepsilon_{\varphi z} \end{bmatrix} dA\, dz\, dt \tag{29}$$

Replacing the strain components from (7) in (29) gives:
The strain energy variation corresponding to ε_x is:

$$\iint_A \int_{-h/2}^{h/2} \sigma_x \delta\varepsilon_x \, dA\, dz = -\iint_A \left[\frac{\partial N_x}{\partial x} \delta u_0 + \frac{\partial M_x}{\partial x} \delta\theta_x + \left(\frac{-4}{3h^2}\right) \frac{\partial M_x^*}{\partial x} \delta\theta_x + \left(\frac{-4}{3h^2}\right) \frac{\partial^2 M_x^*}{\partial x^2} \delta w_0 \right] dA \tag{30}$$

The strain energy variation corresponding to ε_φ is:

$$\iint_A \int_{-h/2}^{h/2} \sigma_\varphi \delta\varepsilon_\varphi dA\, dz = -\iint_A \left[\begin{array}{l} \frac{1}{R} \frac{\partial N_\varphi}{\partial \varphi} \delta v_0 + \frac{1}{R} \frac{\partial M_\varphi}{\partial \varphi} \delta\theta_\varphi \\ + \frac{1}{R} \left(\frac{-4}{3h^2}\right) \frac{\partial M_\varphi^*}{\partial \varphi} \delta\theta_\varphi + \frac{1}{R^2} \left(\frac{-4}{3h^2}\right) \frac{\partial^2 M_\varphi^*}{\partial \varphi^2} \delta w_0 - \frac{1}{R^2} \left(\frac{-4}{3h^2}\right) \frac{\partial M_\varphi^*}{\partial \varphi} \delta v_0 - \frac{1}{R} N_\varphi \delta w_0 \end{array} \right] dA \tag{31}$$

The strain energy variation corresponding to $\varepsilon_{\varphi x}$ is:

$$\iint_A \int_{-h/2}^{h/2} \sigma_{x\varphi} \delta\varepsilon_{\varphi x} dA\, dz = -\iint_A \left[\frac{1}{R} \frac{\partial N_{\varphi x}}{\partial \varphi} \delta u_0 + \frac{1}{R} \frac{\partial M_{\varphi x}}{\partial \varphi} \delta\theta_x + \frac{1}{R} \left(\frac{-4}{3h^2}\right) \frac{\partial M_{\varphi x}^*}{\partial \varphi} \delta\theta_x + \frac{1}{R} \left(\frac{-4}{3h^2}\right) \frac{\partial^2 M_{\varphi x}^*}{\partial x\, \partial \varphi} \delta w_0 \right] dA \tag{32}$$

The strain energy variation corresponding to $\varepsilon_{x\varphi}$ is:

$$\iint_A \int_{-h/2}^{h/2} \sigma_{\varphi x} \delta\varepsilon_{x\varphi} dA\, dz = -\iint_A \left[\begin{array}{l} \frac{\partial N_{x\varphi}}{\partial x} \delta v_0 + \frac{\partial M_{x\varphi}}{\partial x} \delta\theta_\varphi \\ + \frac{-4}{3h^2} \frac{\partial M_{x\varphi}^*}{\partial x} \delta\theta_\varphi + \frac{-4}{3h^2} \frac{1}{R} \frac{\partial^2 M_{x\varphi}^*}{\partial x\, \partial \varphi} \delta w_0 + \frac{-4}{3h^2} \left(-\frac{1}{R}\right) \frac{\partial M_{x\varphi}^*}{\partial x} \delta v_0 \end{array} \right] dA \tag{33}$$

The strain energy variation corresponding to ε_{xz} is:

$$\iint_A \int_{-h/2}^{h/2} \sigma_{xz} \delta\gamma_{xz} dA\, dz = -\iint_A \left[-Q_x \delta\theta_x - 3\left(\frac{-4}{3h^2}\right) Q_x^* \delta\theta_x + 3\left(\frac{-4}{3h^2}\right) \frac{\partial Q_x^*}{\partial x} \delta w_0 + \frac{\partial Q_x}{\partial x} \delta w_0 \right] dA \tag{34}$$

The strain energy variation corresponding to $\varepsilon_{\varphi z}$ is:

$$\iint_A \int_{-h/2}^{h/2} \sigma_{\varphi z} \delta\gamma_{\varphi z} dA\, dz = -\iint_A \left[-R_\varphi \delta\theta_\varphi - 3\left(\frac{-4}{3h^2}\right) R_\varphi^* \delta\theta_\varphi + 3\left(\frac{-4}{3h^2}\right) \frac{1}{R} \frac{\partial R_\varphi^*}{\partial \varphi} \delta w_0 + \frac{1}{R} \frac{\partial Q_\varphi}{\partial \varphi} \delta w_0 + \frac{1}{R} Q_\varphi \delta v_0 - 3\left(\frac{-4}{3h^2}\right)\left(-\frac{1}{R}\right) R_\varphi^* \delta v_0 \right] dA \tag{35}$$

In addition to (29)-(34), it is required to add strain energy variations such as the initial stress δU^i to the shell strain energy variation in (21) to incorporate initial stresses in the governing equations. Thus, the energy variations, such as initial stresses, are written as [20, 21]:

$$\delta U^{i} = \delta \iint_{A} \int_{-h/2}^{h/2} \left[\sigma_x^i \varepsilon_{x0} + \sigma_\varphi^i \varepsilon_{\varphi 0} + \sigma_{x\varphi}^i \gamma_{x\varphi 0} \right] R\,dx\,d\varphi\,dz \tag{36}$$

where σ_x^i, σ_φ^i, and $\sigma_{x\varphi}^i$ are the initial axial, circumferential, and torsional stresses, respectively. The shell is assumed to be in equilibrium under this initial stress field. The potential energy of the shell under the initial stresses is treated as the reference energy level in dynamic shell analysis. As the shell may be subject to high initial stresses, it is required to include not only the linear strain terms but also the nonlinear second-order strain terms imposing large deformations in (36). This gives integral terms good convergence in terms of the order in comparison to integral terms in (21) [20, 21]. The strains with nonlinear terms are written as [20, 22]

$$\begin{aligned}
\varepsilon_{x0} &= \frac{\partial u_0}{\partial x} + \frac{1}{2}\left[(\frac{\partial u_0}{\partial x})^2 + (\frac{\partial v_0}{\partial x})^2 + (\frac{\partial w_0}{\partial x})^2 \right] \\
\varepsilon_{\varphi 0} &= \frac{1}{R}\frac{\partial v_0}{\partial \varphi} + \frac{1}{R}w + \frac{1}{2R^2}\left[(\frac{\partial u_0}{\partial \varphi})^2 + (\frac{\partial v_0}{\partial \varphi} + \mathrm{w}_0)^2 + (\frac{\partial w_0}{\partial \varphi} - v_0)^2 \right] \\
\gamma_{x\varphi 0} &= \frac{\partial v_0}{\partial x} + \frac{1}{R}\frac{\partial u_0}{\partial \varphi} + \frac{1}{R}\left[\frac{\partial u_0}{\partial x}\frac{\partial u_0}{\partial \varphi} + \frac{\partial v_0}{\partial x}(\frac{\partial v_0}{\partial \varphi} + \mathrm{w}_0) + \frac{\partial w_0}{\partial x}(\frac{\partial w_0}{\partial \varphi} - v_0) \right]
\end{aligned} \tag{37}$$

Replacing strains from (37) in (36) and defining forces resulting from initial axial, circumferential, and torsional stresses N_x^i, N_φ^i, and $N_{x\varphi}^i$ gives:

$$(N_x^i, N_\varphi^i, N_{x\varphi}^i) = \int_{-h/2}^{h/2} (\sigma_x^i, \sigma_\varphi^i, \sigma_{x\varphi}^i)\,\mathrm{dz} \tag{38}$$

N_x^i, N_φ^i, and $N_{x\varphi}^i$ are assumed to remain unchanged across the shell [20]. Thus,

$$\begin{aligned}
&\delta U^{i} = \delta \iint_{A} \int_{-h/2}^{h/2} \left[\sigma_x^i \varepsilon_{x0} + \sigma_\varphi^i \varepsilon_{\varphi 0} + \sigma_{x\varphi}^i \gamma_{x\varphi 0} \right] R\,dx\,d\varphi\,dz \\
&= -\iint_{A} \left((N_x^i \frac{\partial^2 u_0}{\partial x^2})\delta \mathrm{u}_0 + (N_x^i \frac{\partial^2 v_0}{\partial x^2})\delta v_0 + (N_x^i \frac{\partial^2 w_0}{\partial x^2})\delta w_0 \right) R\,dx\,d\varphi \\
&-\iint_{A} \begin{pmatrix} -(N_\varphi^i \frac{1}{R})\delta \mathrm{w}_0 + (N_\varphi^i \frac{1}{R^2}\frac{\partial^2 u_0}{\partial \varphi^2})\delta u_0 + (N_\varphi^i \frac{1}{R^2}\frac{\partial^2 v_0}{\partial \varphi^2})\delta v_0 \\ -(N_\varphi^i \frac{1}{R^2}\mathrm{w}_0)\delta w_0 - (N_\varphi^i \frac{2}{R^2}\frac{\partial v_0}{\partial \varphi})\delta w_0 + (N_\varphi^i \frac{2}{R^2}\frac{\partial w_0}{\partial \varphi})\delta v_0 \\ +(N_\varphi^i \frac{1}{R^2}\frac{\partial^2 w_0}{\partial \varphi^2})\delta w_0 - (N_\varphi^i \frac{1}{R^2}\mathrm{v}_0)\delta v_0 \end{pmatrix} R\,dx\,d\varphi \\
&-\iint_{A} \begin{pmatrix} (N_{x\varphi}^i \frac{2}{R}\frac{\partial^2 u_0}{\partial x\,\partial \varphi})\delta u_0 + (N_{x\varphi}^i \frac{2}{R}\frac{\partial^2 v_0}{\partial x\,\partial \varphi})\delta v_0 - (N_{x\varphi}^i \frac{2}{R}\frac{\partial v_0}{\partial x})\delta w_0 \\ (N_{x\varphi}^i \frac{2}{R}\frac{\partial w_0}{\partial x})\delta v_0 + (N_{x\varphi}^i \frac{2}{R}\frac{\partial w_0}{\partial x\,\partial \varphi})\delta w_0 \end{pmatrix} R\,dx\,d\varphi
\end{aligned} \tag{39}$$

The initial stresses are typically assumed to carry a membrane nature – i.e., initial stress is treated as uniform and constant in the thickness direction. Thus, for integral terms in (39), only linear terms linking curve variations to displacement components are required to remain in the equations [20, 21].

3.5.2 Deriving equilibrium equations for an integrated composite shell and equations of boundary conditions

Once the work and energy expressions in Hamilton's principle are calculated, shell equilibrium equations can be derived. Based on the fundamental theorem of the calculus of variations, the total values of δu_0, δv_0, δw_0, $\delta\theta_x$, and $\delta\theta_\varphi$ in double integrals in (26), (27), (30)-(35), and (39) must be equal to zero. Then, the boundary condition equations at x=0 and x=L become:

$$\delta u_0 = 0; \qquad N_x - \hat{N}_x = 0 \tag{40}$$

$$\delta v_0 = 0; \qquad \left(N_{x\varphi} + \frac{1}{R} M_{x\varphi}\right) - \left(\hat{N}_{x\varphi} + \frac{1}{R}\hat{M}_{x\varphi}\right) = 0 \tag{41}$$

$$\delta w_0 = 0; \qquad Q_x - \hat{Q}_x = 0 \tag{42}$$

$$\delta\theta_x = 0; \qquad M_x - \hat{M}_x = 0 \tag{43}$$

$$\delta\theta_\varphi = 0; \qquad M_{x\varphi} - \hat{M}_{x\varphi} = 0 \tag{44}$$

where $\hat{N}_x$, $\hat{M}_{x\varphi}$, $\hat{Q}_x$, and $\hat{M}_x$ are loads on the shell's edges. However, axial and circumferential preloads were employed due to the analysis conditions.

3.5.3 Deriving differential operators

To solve the equilibrium equations, strain values must be placed in (15) by the strain-displacement relations in (7). Then, the resultant relations are placed in the equilibrium equations.

3.5.4 Analyzing the free vibration of composite shells

The boundary conditions must be applied to the displacement components via functions. The simple boundary conditions are defined as [15]:

$$v_0 = w_0 = \theta_x = N_x = M_x = M_x^* = 0 \tag{45}$$

To meet conditions in (45), the displacement components are considered in extended coordinate $T_{mn}(t)$ as [23, 24]

$$\begin{aligned} u_0 &= u_{0mn} \cos\lambda x \cos n\varphi \, e^{iw_{mn}t} \\ v_0 &= v_{0mn} \sin\lambda x \sin n\varphi \, e^{iw_{mn}t} \\ w_0 &= w_{0mn} \sin\lambda x \cos n\varphi \, e^{iw_{mn}t} \\ \theta_x &= \theta_{xmn} \cos\lambda x \cos n\varphi \, e^{iw_{mn}t} \\ \theta_\varphi &= \theta_{\varphi mn} \sin\lambda x \sin n\varphi \, e^{iw_{mn}t} \end{aligned} \tag{46}$$

where $\lambda = m\pi/L$, $T_{mn}(t) = e^{i\omega_{mn}t}$, u_{0mn}, v_{0mn}, w_{0mn}, θ_{xmn}, and $\theta_{\varphi mn}$ are the natural mode shapes. Then, the differential operators are written as:

$$\begin{bmatrix} L_{1,1} & L_{1,2} & L_{1,3} & L_{1,4} & L_{1,5} \\ L_{2,1} & L_{2,2} & L_{2,3} & L_{2,4} & L_{2,5} \\ L_{3,1} & L_{3,2} & L_{3,3} & L_{3,4} & L_{3,5} \\ L_{4,1} & L_{4,2} & L_{4,3} & L_{4,4} & L_{4,5} \\ L_{5,1} & L_{5,2} & L_{5,3} & L_{5,4} & L_{5,5} \end{bmatrix} \tag{47}$$

Replacing natural mode shape vector Δ in the differential operators gives:

$$L_{ij}(\Delta) = 0 \tag{48}$$

The Galerkin method was employed to solve the equation system as [25,26]:

$$\int_0^b \int_0^a L_{ij}(\Delta) T_{mn}(t) \psi dx dy = 0 \tag{49}$$

where L_{ij} is a differential operator in which the displacement components are replaced. Also, ψ is the weight function vector represented as:

$$\psi = \begin{bmatrix} \cos\lambda x \cos n\varphi \\ \sin\lambda x \sin n\varphi \\ \sin\lambda x \cos n\varphi \\ \cos\lambda x \cos n\varphi \\ \sin\lambda x \sin n\varphi \end{bmatrix}, \ \Delta = \begin{bmatrix} u_{0mn} \cos\lambda x \cos n\varphi \\ v_{0mn} \sin\lambda x \sin n\varphi \\ w_{0mn} \sin\lambda x \cos n\varphi \\ \theta_{xmn} \cos\lambda x \cos n\varphi \\ \theta_{\varphi mn} \sin\lambda x \sin n\varphi \end{bmatrix} \tag{50}$$

Solving (48) gives an eigenvalue equation as:

$$\left[K - \omega_{mn}^2 M\right] d = 0 \tag{51}$$

In which

$$d = \begin{bmatrix} u_{0mn} & v_{0mn} & w_{0mn} & \theta_{xmn} & \theta_{\varphi mn} \end{bmatrix}^T \tag{52}$$

Solving (52) yields the eigenvalues of the natural frequencies and their corresponding mode shapes – the smallest natural frequency is the square root of the smallest eigenvalue. To obtain the eigenvalues, matrixes *M* and *K* are placed in (51), and the natural frequencies are calculated in MATLAB.

3.5.5 Defining stiffness distribution and mass distribution via the Heaviside step function to analyze perforated cylindrical shells

Due to the different materials of rips and fillers in perforated shells, no uniform stiffness distribution can be employed. Thus, such a distribution is performed using the Heaviside step function as [27]:

$$Q_{ij}(x,y) = Q_{ij}^{rib}[1 - HP(x,y)] + Q_{ij}^{bay} HP(x,y) \tag{53}$$

$$\rho(x,y) = \rho^{rib}[1 - HP(x,y)] + \rho^{bay} HP(x,y) \tag{54}$$

where $y = R\varphi$ and $Q_{ij}(x,y)$ is the general stiffness, Q_{ij}^{rib} is the rib stiffness, Q_{ij}^{bay} is the filler stiffness, $HP(x,y)$ is the distribution function, $\rho(x,y)$ is the general density, ρ^{rib} is the rib density, and ρ^{bay} is the filler density. The distribution function is 0 on ribs and 1 on fillers. Thus,

$$HP(x,y)=\begin{cases}1 & between\ \ ribs\\ 0 & on\ \ ribs\end{cases} \tag{55}$$

Fig. 2 illustrates the Heaviside step function along a cylinder with two cavities.

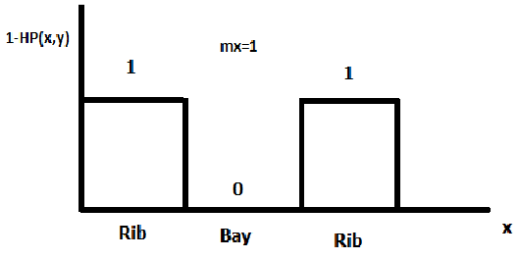

Fig.2
The Heaviside step function along a cylinder with two cavities.

For an orthogrid-reinforced structure, the Heaviside distribution is written as [27]:

$$HP(x,\mathrm{y})=\sum_{i=1}^{m_x}\sum_{j=1}^{n_y}[H(x-x_i+\frac{h_{bxi}}{2})-H(x-x_i-\frac{h_{bxi}}{2})]\times[H(\mathrm{y}-y_j+\frac{h_{bxi}}{2})-H(\mathrm{y}-y_j-\frac{h_{byj}}{2})] \tag{56}$$

If the perforated structure contains orthotropic ribs, vertical, horizontal, and diagonal ribs with fillers are analyzed as:

$$Q_{ij}=Q_{ij}^{0}(1-HP^{0})+Q_{ij}^{90}(1-HP^{90})+Q_{ij}^{bay}(HP^{0}\times HP^{90}) \tag{57}$$

$$\rho=\rho^{0}(1-HP^{0})+\rho^{90}(1-HP^{90})+\rho^{bay}(HP^{0}\times HP^{90}) \tag{58}$$

$$\begin{aligned}
HP^{0}&=\sum_{i=1}^{m_x}\sum_{j=1}^{m_y}\left[H(\mathrm{y}-y_j+\frac{h_{bxi}}{2})-H(\mathrm{y}-y_j-\frac{h_{byj}}{2})\right]\\
HP^{90}&=\sum_{i=1}^{m_x}\sum_{j=1}^{m_y}\left[H(x-x_i+\frac{h_{bxi}}{2})-H(x-x_i-\frac{h_{bxi}}{2})\right]\\
HP^{\varphi}&=\sum_{i=1}^{m_x}\sum_{j=1}^{m_y}\left[H(x-x_i+\frac{h_{\varphi x}}{2})-H(x-x_i-\frac{h_{\varphi x}}{2})\right]\times\left[H(\mathrm{y}-y_j+\frac{h_{\varphi y}}{2})-H(\mathrm{y}-y_j-\frac{h_{\varphi y}}{2})\right]\\
HP^{-\varphi}&=\sum_{i=1}^{m_x}\sum_{j=1}^{m_y}\left[H(x-x_i+\frac{h_{-\varphi x}}{2})-H(x-x_i-\frac{h_{-\varphi x}}{2})\right]\times\left[H(\mathrm{y}-y_j+\frac{h_{-\varphi y}}{2})-H(\mathrm{y}-y_j-\frac{h_{-\varphi y}}{2})\right]
\end{aligned} \tag{59}$$

where x_i and y_j denote the coordinates of each cell's center, h is the rib thickness, and $m_x \times n_y$ represents the number of cells. Also,

$$x_i,\ i=1,\ldots,m_x \qquad y_i,\ j=1,\ldots,n_y \tag{60}$$

3.5.6 Deriving differential operators for perforated shells

The equations governing perforated cylindrical shells are derived in the same way as those of non-perforated composite shells. In replacing the resultant stresses in Euler equations and deriving differential operators, it should be noted that the entries of matrix D vary with respect to x and y and are included in differentiation due to the Heaviside step function, unlike non-perforated shells. Thus, the differentials are included in the calculations from (56) and (59). Once the entire differential operators are obtained as described, the remaining steps of obtaining natural frequencies will be the same as those of typical composite shells. The first differential operator in composite shells is defined as:

$$\begin{aligned} L_{11} &= D_{m(1,1)}\frac{\partial^2 u_0}{\partial x^2} + D_{m(1,3)}\frac{1}{R}\frac{\partial^2 u_0}{\partial x\,\partial y} + D_{m(3,1)}\frac{1}{R}\frac{\partial^2 u_0}{\partial x\,\partial y} + \frac{1}{R}D_{m(3,3)}\frac{1}{R}\frac{\partial^2 u_0}{\partial y^2} \\ &\underline{\frac{\partial D_{m(1,1)}}{\partial x}\frac{\partial u_0}{\partial x} + \frac{\partial D_{m(1,3)}}{\partial x}\frac{1}{R}\frac{\partial u_0}{\partial y} + \frac{\partial D_{m(3,1)}}{\partial y}\frac{1}{R}\frac{\partial u_0}{\partial x} + \frac{1}{R}\frac{\partial D_{m(3,3)}}{\partial y}\frac{1}{R}\frac{\partial u_0}{\partial y} - I_0\frac{\partial^2 u_0}{\partial t^2}} \end{aligned} \tag{61}$$

In which underlined terms are added to the operators of an integrated shell due to the presence of differentials in the entries of matrix D of a perforated shell.

3.5.7 Normalizing mode shapes

An important property of vibration modes in cylindrical shells is their orthogonality to mass and stiffness matrixes. The orthogonality of mode shapes to the mass matrix in a shell is defined as [28]:

$$\int_0^L \int_0^{2\pi} \Delta_{mn}^T M\, \Delta_{ij}\, dx\, d\varphi = \begin{cases} =0 & if \quad m \neq i \quad or \quad n \neq j \\ \neq 0 & if \quad m = i \quad or \quad n = j \end{cases} \tag{62}$$

In which Δ_{mn} is the natural mode shape vector defined in (50). Then, the normalized mode shapes with respect to the mass matrix as calculated as:

$$\int_0^L \int_0^{2\pi} \Delta_{mn}^T M\, \Delta_{mn}\, dx\, d\varphi = 1 \tag{63}$$

As a result, the normalized natural mode shape vector is obtained.

4 RESULTS AND DISCUSSION

The properties of the material are assigned as a composite layup. In modeling by Abacus software, the element SC8R has been used Which is a cubic element with 8 nodes and 6 degrees of freedom. Armenakas et al. (1969) studied the natural frequencies of cylindrical shells by a 3D elasticity theory-based exact solution [29]. Their frequency parameter was defined as:

$$\overline{\omega} = \omega h / \pi\sqrt{\rho/\mathrm{G}} \tag{64}$$

where ω is the natural frequency, h is the shell thickness, ρ is the density, and G is the shear modulus. Table 1 compares the frequencies of a hollow cylinder between the proposed higher-order theory and those of other studies at different h/L and h/R ratios and different circumferential mode numbers. As can be seen, the proposed theory was satisfactorily accurate, as compared to other works. Accurate investigation indicates that a rise in the h/L ratio raises the frequency parameter. Also, an increase in mode number n from 1 to 2 enhanced the frequency parameter. It

should be noted that the results of the MRTSDT and RTSDT were consistent, and the differences between the two theories arise from the use of the trapezoidal coefficient and a higher order in the strain-displacement definition in MRTSDT. Figs. 3 and 4 show the variations of the lowest natural frequency at different *h/R* ratios.

Fig. 3 indicates the variations at the *L/R* ratios of 5 and 10, and Fig. 4 demonstrates the variations at the *L/R* ratios of 15 and 20 for MRTSDT and RTSDT. As can be seen, the difference between the two theories increases as the *h/R* and *L/R* ratios rise. At *h/R*=0 and *L/R*=20, the difference is 2.7%. This can be attributed to the higher number of calculated terms in MRTSDT than in the RTSDT theory.

Table 1
Comparing the lowest frequencies of different theories for an isotropic cylinder.

h/R=0.01	*h/L*	MRTSDT	RTSDT	Hasheminejad [30]	Loy and Lam [31]
n=1	0.1	0.0428	0.0429	0.0314	0.0315
	0.2	0.1154	0.1159	0.1102	0.1102
	0.4	0.3145	0.3159	0.3250	0.3250
	0.6	0.5392	0.5411	0.5591	0.5492
	0.8	0.7717	0.7739	0.7944	0.7944
	1.0	1.0070	1.0092	1.0272	1.0273
n=2	0.1	0.6091	0.6140	0.7175	0.7181
	0.2	0.6091	0.6222	0.7149	0.7156
	0.4	0.6700	0.6726	0.7463	0.7469
	0.8	0.9359	0.9364	0.9936	0.9941
	1.0	1.1236	1.1239	1.1735	1.1741

*difference percentage=((MRTSDT-[20])/[20])*100

Fig. 5 indicates the lowest frequency parameter versus the *L/R* ratio. As mentioned, a rise in the *L/R* ratio reduces the frequency parameter. Moreover, this reduction trend declines as the *L/R* ratio diminishes. It should be noted that the proposed MRTSDT and the RTSDT exhibited close results for isotropic shells.

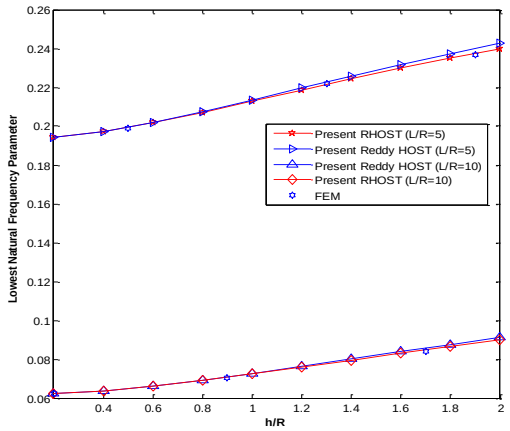

Fig.3
The lowest frequency parameter versus the *h/R* ratio at different *L/R* ratios.

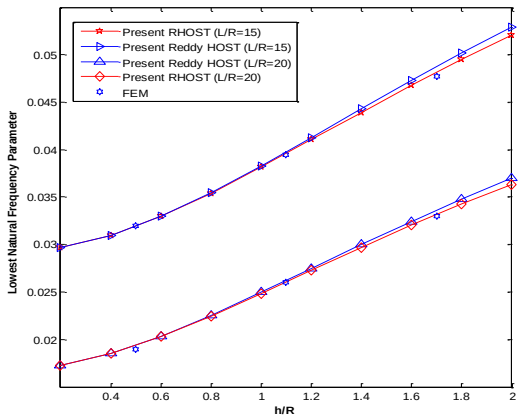

Fig.4
The lowest frequency parameter versus the *h/R* ratio at different *L/R* ratios.

Table 2 compares frequency parameter results for a hollow cylinder with asymmetric orthogonal layer arrangement (0/90/0) at the first six frequency modes, the *L/R* ratio of 2, *h/R* ratio of 0.0025, and different orthotropic ratios to the results of Xie et al. [32]. As can be seen, a rise in the orthotropic ratio increases the frequency parameter. However, the increase rate diminishes as the orthotropic ratio continues to rise. MRTSDT and RTSDT are in good agreement. However, the MRTSDT results are closer to [32] in the entire cases.

Table 3 compares the frequency parameter results of a hollow cylinder with symmetric orthogonal layer arrangement (0/90/0) at the first six frequency modes, the *h/R* ratio of 0.0025, and different *L/R* ratios to those of Xie et al. [32]. According to Table 3, an increase in the *L/R* ratio diminishes the frequency parameter. The maximum difference can be indicated to be 4.45% at a high *L/R* ratio and the 6^{th} mode. It should be noted that MRTSDT suggests that an increase in the number of strain-stress terms at a high mode number reports closer results to the reference, as mentioned in the equations.

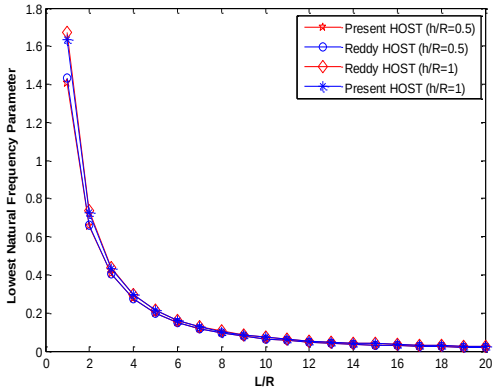

Fig.5
The lowest frequency parameter versus the *L/R* ratio at different *h/R* ratios.

Fig. 6 illustrates the frequency parameter versus the *h/R* ratio at different *L/R* ratios. According to Fig. 6, an enhancement in the *h/R* ratio enhances the frequency parameter. As can be seen, a rise in the *L/R* ratio from 1 to 5 diminishes the incremental slope of the frequency parameter. The parameter frequency became 3.15, 2.83, 2.11, 2.01, and 1.77 times larger as the *h/R* ratio enhanced by three times at the *L/R* ratios of 1, 2, 3, 4, and 5, respectively. Fig. 7 demonstrates the effect of a rise in the mode number on the lowest frequency parameter at different *L/R* ratios. According to Fig. 7, at low mode numbers, the lowest frequency parameter rises as the *L/R* ratio declines. However, the frequency parameter becomes almost the same at different *L/R* ratios as the mode number increases to 10. According to the values obtained at the *L/R* ratios of 1, 2, 5, and 10, the frequency parameter reduces and then begins to increase as the mode number increases from 1 to 10. It should be noted that the base mode number diminishes as the *L/R* ratio rises. This is an essential criterion of designing mechanical, particularly composite, structures.

Table 2
Comparing the frequency parameter for symmetric orthogonal layer arrangement (0/90/0) in a multi-layered cylinder at different E_1/E_2 ratios and the first six bending vibration modes; *h/R*=0.01 and $\omega^* = \omega(R)\sqrt{\rho/E_2}$.

			E_1/E_2 =2.5			
n	1	2	3	4	5	6
MRTSDT	0.0852	0.0305	0.0155	0.0125	0.0158	0.0221
RTSDT	0.0852	0.0305	0.0155	0.0126	0.0159	0.0222
Xie et al. [32]	0.0839	0.0300	0.0151	0.0121	0.0152	0.0211
			E_1/E_2 =5			
n	1	2	3	4	5	6
MRTSDT	0.1036	0.0285	0.0101	0.0148	0.0169	0.0229
RTSDT	0.0103	0.0396	0.0201	0.0148	0.0170	0.0230
Xie et al. [32]	0.1028	0.0392	0.0198	0.0145	0.0164	0.0221
			E_1/E_2 =15			
n	1	2	3	4	5	6
MRTSDT	0.1318	0.0587	0.0310	0.0211	0.0210	0.0266
RTSDT	0.1318	0.0587	0.0310	0.0212	0.0211	0.0268
Xie et al. [32]	0.1316	0.0585	0.0309	0.0209	0.0206	0.0260

Table 3
Comparing the frequency parameter for symmetric orthogonal layer arrangement (0/90/0) in a multi-layered cylinder at different *L/R* ratios and first six bending vibration modes; $\omega^* = \omega(R)\sqrt{\rho/E_2}$.

$m = 1, h/R = 0.002, G_{12} = G_{13} = 0.26E_2, G_{23} = 0.5E_2, \nu_{12} = \nu_{13} = \nu_{23} = 1, E_2/E_3 = 1, E_1/E_2 = 2.5$

	n=1				*n*=2				*n*=3			
L/R	MRTSDT	HRTSDT	Xie et al. [32]	*Difference (%)	MRTSDT	HRTSDT	Xie et al. [32]	Difference	MRTSDT	HRTSDT	Xie et al. [32]	Difference (%)
1	1.0832	1.0932	1.0612	2.0708	0.8184	0.8184	0.8040	1.7914	0.6084	0.6084	0.5973	1.6920
5	0.2518	0.2518	0.2486	1.2876	0.1090	0.1090	0.1072	1.7126	0.0561	0.0561	0.0550	1.8334
10	0.0852	0.0852	0.0839	1.592	0.0305	0.0305	0.0300	1.8349	0.0155	0.0155	0.0151	2.0948
20	0.0240	0.240	0.235	1.7898	0.0080	0.0080	0.0079	1.9487	0.0060	0.0061	0.0085	3.4235
	n=4				*n*=5				*n*=6			
1	0.4577	0.4576	0.4501	1.6752	0.3510	0.3510	0.3452	1.6961	0.2754	0.2754	0.2707	1.7399
5	0.344	0.0345	0.0337	2.0322	0.0264	0.0265	0.0257	2.6732	0.0268	0.0269	0.0258	3.8512
10	0.0125	0.0126	0.0121	3.2211	0.0158	0.0159	0.0152	4.1299	0.0221	0.0222	0.0211	4.3785
20	0.0094	0.0095	0.0090	4.3199	0.0148	0.0150	0.0142	4.4395	0.0217	0.0218	0.0208	4.4579

*difference ratio: ((MRTSDT-[32])/32)*100

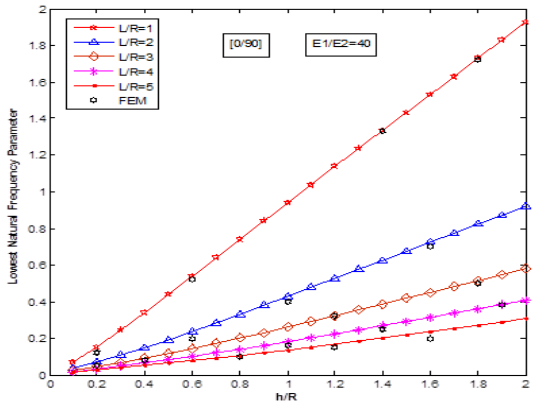

Fig.6
The lowest frequency parameter versus the *h/R* ratio at different *L/R* ratios.

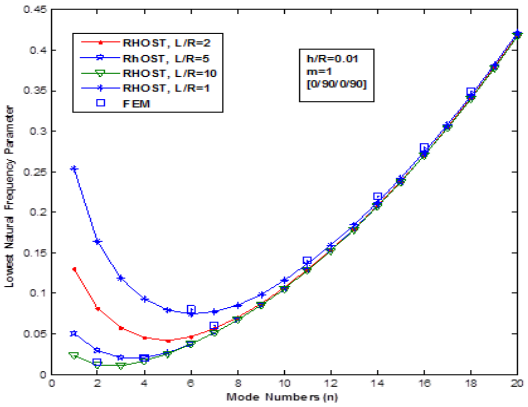

Fig.7
The lowest frequency parameter versus the circumferential mode number at different *L/R* ratios and $E_1/E_2 = 40$.

Table 4 provides the results of the proposed theory along with FEM results for different perforated shell thicknesses and mode shapes. As can be seen, an increase in the grid structure thickness increases the natural frequencies. This can be attributed to the increased stiffness due to the increased thickness. The difference between the proposed theory and the FEM results seems to be acceptable, considering that the theory is a new idea. The

maximum difference of 12.00% occurred in the first mode at an h/R ratio of 0.3. Also, very close results to the FEM results were obtained in the second mode. The differences were 4.30% and 2.79% at an h/R ratio of 0.1 in the second and third modes, respectively. Higher shell thickness and the thick wall analysis could be an explanation for the higher difference between the proposed theory and the FEM results.

Table 4
Comparing the base natural frequency in Hz to the FEM results at different h/R ratios and in different bending vibration mode numbers.

Mode	Theory	h/R=0.1	*Difference (%)	h/R=0.2	Difference (%)	h/R=0.3	Difference (%)
(1, 1)	MRTSDT	28.68	6.94	28.80	9.80	29.09	12.0
	FEM	30.82		31.93		33.06	
Mode Shape				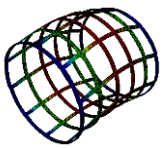		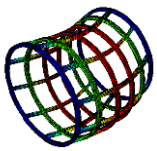	
(1, 2)	MRTSDT	52.72	4.30	53.80	6.12	55.72	7.13
	FEM	55.09		57.31		60.00	
Mode Shape		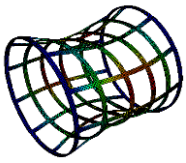		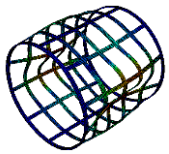		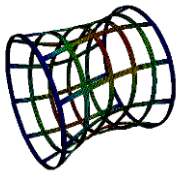	
(3, 1)	MRTSDT	80.70	2.79	84.60	6.10	90.65	7.51
	FEM	83.02		91.10		98.02	
Mode Shape		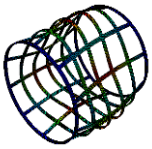		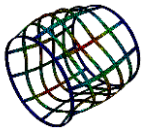		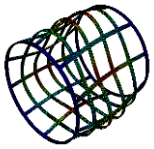	

*Difference percentage: ((MRTSDT-FEM)/FEM)/100, L/R=2, E_1/E_2=40.

Fig. 8 represents the effect of a compressive axial load along with a tensile circumferential load on the natural frequency. The present analysis suggests that an enhancement in the initial stresses has an essential effect on the natural frequency, in that it reduces the natural frequency. According to the results, the difference between the MRTSDT and RTSDT results becomes very small under different axial and circumferential loads. The difference is more clearly seen at S=-1. This can be attributed to the effect of the trapezoidal form factor on circumferential results. Finally, the natural frequency is minimized at critical and buckling loads.

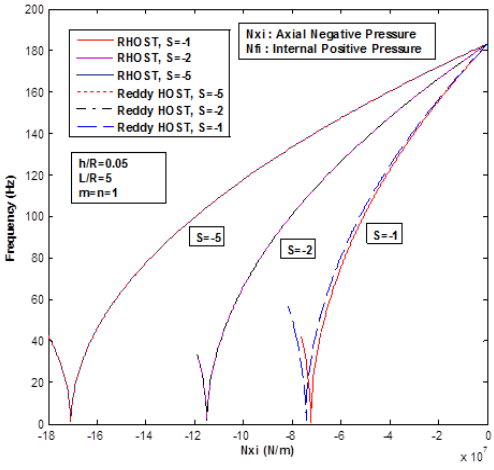

Fig.8
The lowest natural frequency in Hz under an initial axial and circumferential load with 10 circumferential grids and 5 longitudinal grids.

5 CONCLUSIONS

1. The proposed MRTSDT was satisfactorily accurate in comparison to RTSDT in which the trapezoidal effect and higher-order $\gamma_{\varphi z}$ terms were not included. This can specifically be seen in the comparison of the proposed theory and FEM results for cylindrical shells.
2. The more accurate results of the proposed theory than those of different high-order theories implied the positive contribution of the trapezoidal effect and high-order $\gamma_{\varphi z}$ terms.
3. For isotropic cylindrical shells, an enhancement in the *h/L* ratio increases the frequency parameter. Also, MRTSDT exhibited higher accuracy at lower *h/L* ratios.
4. For composite cylindrical shells, I was observed that an increase in the *L/R* ratio diminished the frequency parameter. It was found that the frequency parameter reduction rate increased but then began to diminish as the *L/R* ratio increased in different layer arrangements.
5. The lowest frequency parameter increased as the E_1/E_2 ratio increased in different composite layer arrangements. The variation of the frequency parameter diminished at higher E_1/E_2 rations. Also, the proposed theory exhibited higher accuracy.
6. The lowest frequency reduced as the *h/R* ratio enhanced. Also, according to the results, the proposed theory was closer to RTSDT at lower *h/R* ratios and approximated the frequencies slightly lower than their real values at higher h/R ratios.
7. As the circumferential mode number of a composite cylindrical shell increased, the frequency parameter reduced and then began to increase.
8. A rise in the initial axial and circumferential stresses with different rations diminished the natural frequency. In this case, the results of the two theories were in good agreement.

REFERENCES

[1] Hideo T., 1991, Static analyses of elastic plates with voids, *International Journal of Solids and Structures* **28**: 179-196.

[2] Hideo T., 1991, Dynamic analyses of elastic plates with voids, *International Journal of Solids and Structures* **28**: 879-895.

[3] De-Chih L., Chih-Shiung W., Lin-Tsang L., 2011, The natural frequency of elastic plates with void by ritz-method, *Studies in Mathematical Sciences* **2**: 36-50.

[4] Huybrechts S., Tsai S.W., 1996, Analysis and behavior of grid structures, *Composites Science and Technology* **56**: 1001-1015.

[5] Huybrechts S.M., 2002, Manufacturing theory for advanced grid stiffened structures, *Composites Part A: Applied Science and Manufacturing* **33**: 155-161.

[6] Han D., Tsai S.W., 2003, Interlocked composite grids design and manufacturing, *Journal of Composite Materials* **37**: 287-316.

[7] Jiang J., Olson M., 1994, Vibration analysis of orthogonally stiffened cylindrical shells using super finite elements, *Journal of Sound and Vibration* **173**: 73-83.

[8] Hemmatnezhad M., Rahimi G., Ansari R., 2014, On the free vibrations of grid-stiffened composite cylindrical shells, *Acta Mechanica* **225**: 609-623.

[9] Luan Y., Ohlrich M., Jacobsen F., 2011, Improvements of the smearing technique for cross-stiffened thin rectangular plates, *Journal of Sound and Vibration* **330**: 4274-4286.

[10] Edalata P., Khedmati M.R., Soares C.G., 2013, Free vibration and dynamic response analysis of stiffened parabolic shells using equivalent orthotropic shell parameters, *Latin American Journal of Solids and Structures* **10**: 747-766.

[11] Eskandari Jam J., Nouradbadi M., Taghavian S., 2011, Designing a non-isotropic perforated conical structure, *International Conference of Composites*, Iran University of Science and Technology.

[12] Nourabadi M., Taghavian S., 2010, Designing a non-isotropic conical perforated structure, *The 2nd International Conference of Composites*, Iran University of Science and Technology.

[13] Sayyad K., 2011, Analyzing the inter-layer shear effect on the local buckling of a perforated polymer composite cylinder under compressive axia loading, *The 10th Conference of Iran Aerospace Association*.

[14] Liew K., Lim C., 1996, A higher-order theory for vibration of doubly curved shallow shells, *Journal of Applied Mechanics* **63**: 587-593.

[15] Garg A.K., Khare R.K., Kant T., 2006, Higher-order closed-form solutions for free vibration of laminated composite and sandwich shells, *Journal of Sandwich Structures and Materials* **8**: 205-235.

[16] Reddy J.N.,2004, *Mechanics of Laminated Composite Plates and Shells: Theory and Analysis*, CRC Press.

[17] Reddy J., Liu C., 1985, A higher-order shear deformation theory of laminated elastic shells, *International Journal of Engineering Science* **23**: 319-330.

[18] Bert C.W., 1967, Structural theory for laminated anisotropic elastic shells, *Journal of Composite Materials* **1**: 414-423.
[19] Leissa A., Chang J.-D., 1996, Elastic deformation of thick, laminated composite shells, *Composite Structures* **35**: 153-170.
[20] Davar A., 2010, *Analyzing FML and FGM Cylindrical Shells Under Transverse Impact Loading*, Doctorial Dissertation, K. N. Toosi University of Technology.
[21] Leissa A.W., 1973, *Vibration of Shells*, Nasa SP-288, US Governmet Printing Office, Washington D.C., Reprinted by the Acoustical Society of America.
[22] Amabili M., 2003, A comparison of shell theories for large-amplitude vibrations of circular cylindrical shells: Lagrangian approach, *Sound and Vibration* **264**: 1091-1125.
[23] Kahandani R., 2014, *Analyzing the Free Vibration of Perforated Composite Shells with Two Curvatures by an Extended High-Order Theory*, Master's thesis, Malek-Ashtar University of Technology.
[24] Ye J., Soldatos K., 1994, Three-dimensional vibration of laminated cylinders and cylindrical panels with symmetric or antisymmetric cross-ply lay-up, *Composites Engineering* **4**: 429-444.
[25] Qatu M.S.,2004, *Vibration of Laminated Shells and Plates*, Elsevier.
[26] Reddy J.N., 2002, *Energy Principles and Variational Methods in Applied Mechanics*, John Wiley & Sons.
[27] Li G., Cheng J., 2007, A generalized analytical modeling of grid stiffened composite structures, *Journal of Composite Materials* **41**: 2939-2969.
[28] Meirovitch L., 2001, *Fundamentals of Vibrations*, McGraw-Hill.
[29] Armenàkas A.E., Gazis D.C., Herrmann G., 1969, *Free Vibrations of Circular Cylindrical Shells*, DTIC Document.
[30] Hasheminejad S.M., Mirzaei Y., 2009, Free vibration analysis of an eccentric hollow cylinder using exact 3D elasticity theory, *Journal of Sound and Vibration* **326**: 687-702.
[31] Loy C.T., Lam K.Y., 1999, Vibration of thick cylindrical shells on the basis of three-dimensional theory of elasticity, *Journal of Sound and Vibration* **37**: 226-719.
[32] Xie X., Jin G., Yan Y., Shi S.X., Liu Z., 2014, Free vibration analysis of composite laminated cylindrical shells using the Haar wavelet method, *Composite Structures* **109**: 169-177.
[33] Li X., Zhang W., Yang X-D., Song L.-K., 2019, A unified approach of free vibration analysis for stiffened cylindrical shell with general boundary conditions, *Mathematical Problems in Engineering* **2019**: 1-14.